Oxygen-vacancy-induced 90°-domain clamping in ferroelectric $Bi_4Ti_3O_{12}$ single crystals

Yuuki Kitanaka, Yuji Noguchi, and Masaru Miyayama
Research Center for Advanced Science and Technology, The University of Tokyo, Meguro-ku, Tokyo 153-8904, Japan
(Received 24 December 2009; revised manuscript received 1 March 2010; published 23 March 2010)

We have investigated domain clamping in ferroelectric single crystals of $Bi_4Ti_3O_{12}$ (BiT) and $(Bi_{3.6}La_{0.4})Ti_3O_{12}$ (BLT) using polarization measurements along the $a(b)$ axis and piezoresponse force microscopy (PFM). PFM observations reveal that 90° domains are clamped during polarization switching. The crystals of BiT with less oxygen vacancies and BLT exhibited a low volume fraction of the clamped 90° domains. Polarization measurements demonstrate that the clamping of 90° domains decreases the remanent polarization in BiT crystals. These experimental results and *ab initio* calculations show that an attractive interaction between 90°-domain walls and oxygen vacancies is the main origin of the clamping of 90° domains.

DOI: 10.1103/PhysRevB.81.094114 PACS number(s): 77.80.Dj, 77.84.Cg, 61.72.jd, 85.50.−n

I. INTRODUCTION

The static and dynamic behaviors of ferroelectric domains are the underlying basis of various functional properties of ferroelectric materials, such as dielectricity, piezoelectricity, ferroelectricity, and electro-optic and acoustic-optic effects. Since the performance of ferroelectric devices is governed by these behaviors, various techniques for enhancing device performance have been widely investigated with the aim of controlling ferroelectric domains.[1–4] Such control, however, is often prevented not only by a large leakage current but also by undesirable behaviors such as domain clamping,[5–7] fatigue,[8,9] aging,[10,11] imprinting,[12] and depoling.[8] Ferroelectric devices thus suffer from degraded polarization and poor reliability due to insufficient control over ferroelectric domains.

The phenomenon called "domain clamping," in which ferroelectric domains resist switching and become unswitchable under an applied electric field (E), is known to cause significant problems in ferroelectric memories and piezoelectric devices. Electrically charged defects such as oxygen vacancies, particularly, are thought to cause domain clamping,[6,13–16] that is, to decrease switchable domains, which in turn leads to a low remanent polarization (P_r). Although several explanations have been offered for the mechanism of the interaction between such defects and various kinds of domain walls (DWs), it remains unclear how the behavior of ferroelectric domains is influenced by these defects owing to the difficulty involved in the direct observation of domain dynamics.

Bismuth titanate ($Bi_4Ti_3O_{12}$:BiT), which is a member of bismuth layer-structured ferroelectrics, has been regarded as a promising material for applications involving ferroelectric memories and piezoelectric devices operating at high temperatures due to its large spontaneous polarization (P_s) and high Curie temperature.[17] The crystal structure of BiT consists of an alternate stacking of Bi_2O_2 layers and perovskite $Bi_2Ti_3O_{10}$ layers along the c axis, and its P_s vector lies mainly along the a axis with a small component along the c axis.[17,18] Although BiT possesses the large P_s, BiT-based ceramics and thin films often show poor polarization properties with a low P_r.[19–22] During heat treatment, the vacancies of Bi and O are more or less formed in Bi-based ferroelectric oxides, including BiT. The vacancy formation of BiT at high temperatures[23,24] is expressed by

$$2Bi_{Bi}^{*} + 3O_{O}^{*} \rightarrow 2V_{Bi}''' + 3V_{O}^{\bullet\bullet} + 2Bi(gas) + 3/2O_2(gas), \quad (1)$$

where V_{Bi}''' and $V_{O}^{\bullet\bullet}$ represent vacancies at the Bi site and the O site, respectively. This vacancy formation indicates that the concentration of $V_{O}^{\bullet\bullet}$, $[V_{O}^{\bullet\bullet}]$, is governed by that of V_{Bi}''', $[V_{Bi}''']$, as in the case of $BaTiO_3$,[25–27] in which $[V_{O}^{\bullet\bullet}]$ is mainly determined by the concentration of acceptor impurities. For BiT at high temperatures, the vacancy concentrations have been reported to vary according to oxygen partial pressure (Po_2) while the ratio of $[V_{O}^{\bullet\bullet}]/[V_{Bi}''']$ is fixed at approximately 3/2 due to the charge neutrality restriction.[23,28] These vacancies largely degrade the polarization properties even in bulk single crystals of BiT.[29,30] Since the value of P_r is determined by the volume fraction of switchable domains obtained by applying E, a low P_r is caused by the clamping of the domains. The poor polarization properties observed for BiT single crystals suggest that domain clamping originates not from extrinsic factors such as grain boundaries in ceramics or strain effects of the substrates in thin films but from the vacancies induced in the crystals.

In this paper, we report upon the structure and clamping of ferroelectric domains in BiT and $(Bi_{3.6}La_{0.4})Ti_3O_{12}$ (BLT) single crystals. Piezoresponse force microscopy (PFM) observations provide direct evidence of the clamping of 90° domains during polarization switching. Experimental results and *ab initio* calculations show that an attractive interaction between 90° DWs and oxygen vacancies is the main origin of the clamping of 90° DWs in the BiT system.

II. EXPERIMENTAL PROCEDURE

BiT single crystals were grown by a flux method using BiT powder and excess Bi_2O_3 powder.[29] The BiT crystals obtained were transparent platelike sheets with lateral dimensions of 10×10 mm^2 and a thickness of 0.1–0.2 mm along the c axis. Three grades of BiT crystals with different concentrations of the vacancies of Bi and O were prepared: "standard," "less-defective," and "more-defective" crystals.

TABLE I. Preparation conditions and polarization properties of BiT and BLT crystals.

Crystal	Crystal-growth condition	Defect-formation treatment	Annealing treatment	P_r ($\mu C/cm^2$)	E_c (kV/cm)
Standard BiT	Soaking: 1200 °C 10 h slow cooling: ~1000 °C 40 h in air (Po_2=0.02 MPa)		900 °C 10 h in air (Po_2=0.02 MPa)	43	32
Less-defective BiT	Soaking: 1200 °C 10 h slow cooling: ~1000 °C 40 h in O_2 (Po_2=0.1 MPa)		900 °C 10 h in air (Po_2=0.02 MPa)	45	30
More-defective BiT	Soaking: 1200 °C 10 h slow cooling: ~1000 °C 40 h in air (Po_2=0.02 MPa)	1000 °C 10 h in N_2 ($Po_2=10^{-5}$ MPa)		30	45
BLT	Soaking: 1200 °C 10 h slow cooling: ~1000 °C 40 h in air (Po_2=0.02 MPa)		900 °C 10 h in air (Po_2=0.02 MPa)	36	42

The details of their crystal growth and polarization properties are presented in Table I. The crystals grown in air are denoted as standard BiT crystals. To obtain less-defective BiT crystals, as compared with the standard ones, Po_2 during crystal growth was controlled based on the defect chemistry at high temperatures. The vacancy formation reaction expressed by Eq. (1) is suppressed at a higher Po_2 and is accelerated at a lower Po_2 during heat treatment.[30] This allows us to change the concentrations of the vacancies in BiT crystals by controlling Po_2 during crystal growth. The standard BiT crystals were grown in air (Po_2=0.02 MPa), and the less-defective crystals were grown under an oxygen gas flow, i.e., Po_2=0.1 MPa. Since crystal growth at a higher Po_2 suppresses the vacancy formation reaction, less-defective crystals with lower $[V'''_{Bi}]$ and $[V^{\bullet\bullet}_{O}]$ could be realized, as compared to the standard BiT crystals. To remove the mechanical stress induced during crystal growth, the standard and less-defective crystals were annealed in air at 900 °C for 10 h prior to electrical measurements and domain observation.

To obtain the more-defective crystals, heat treatment in a nitrogen gas flow at a Po_2 of 1×10^{-5} MPa at 1000 °C (nitrogen annealing) was performed on the standard crystals instead of the annealing treatment in air. Hereafter, this heat treatment in nitrogen gas is termed "defect-formation treatment." The results of thermogravimetric analysis[23,28] have shown that vacancy formation [Eq. (1)] occurs above 1000 °C in a nitrogen gas flow. Defect-formation treatment at 1000 °C can introduce vacancies into the standard crystals, thereby producing the more-defective crystals that have a higher $[V'''_{Bi}]$ and $[V^{\bullet\bullet}_{O}]$ than the standard BiT crystals.

We also prepared single crystals of La-substituted BiT $[(Bi_{4-x}La_x)Ti_3O_{12}$:BLT] which were grown in air by using BLT powder and excess Bi_2O_3 powder via a flux method,[31] and then annealed in air at 900 °C. The composition of the BLT crystals was determined to be $(Bi_{3.6}La_{0.4})Ti_3O_{12}$ (x=0.4) by using inductively coupled plasma-atomic emission spectroscopy. The preparation conditions of the BiT and BLT crystals in this study are listed in Table I.

For electrical measurements, the crystals were cut so that the electric field was applied along the $a(b)$ axis. Au electrodes were sputtered onto the cut faces and polarization properties were measured along the $a(b)$ axis. The domain structures of the crystals were observed by a commercial PFM unit (SII SPI3800N). Before the observation of domain structures, bipolar triangular waves with a maximum E of 80–100 kV/cm at a frequency of 1 Hz were applied to the crystals along the $a(b)$ axis at 25 °C as a poling treatment. Since the condition of the poling treatment is the same as that for the measurement of polarization properties, the state of the domain structure observed is equivalent to that of the "$+P_r$" or "$-P_r$" state in the polarization hysteresis loops. After the poling treatment, the crystal surfaces to be observed were mechanically polished and Au electrodes were deposited on opposite surfaces to serve as bottom electrodes for PFM observation. The details of the domain observations conducted with PFM are described in Ref. 32. The PFM images were made from $A\cos\phi$ (PFM signal), where A is the amplitude and ϕ is the phase of the first harmonic signal induced by the inverse piezoelectric effect. The directions of the P_s vectors were determined through analyses of in-plane and out-of-plane PFM signals in each domain. Because the crystal structure of BiT has a monoclinic distortion ($B1a1$ space group) in the ferroelectric state, the P_s vector slightly tilts at an angle of 4°–5° from the a axis to the c axis.[18] In this study, we focus our attention on the major P_s component along the a axis to investigate three-dimensional (3D) domain structure in the crystal because the a-axis component of P_s (~50 $\mu C/cm^2$) is ten times as large as that along the c axis (4 $\mu C/cm^2$).[17]

III. METHOD OF CALCULATION

Ab initio calculations were performed to investigate the interaction between defects such as O vacancies and 90° DWs. Because modeling the 90° domain structure of BiT requires a huge supercell, we chose tetragonal perovskite $PbTiO_3$ as a model material for the calculations. The calculations were conducted using density-functional theory (DFT) via the generalized gradient approximation[33] with a plane-wave-basis set. The projector-augmented wave method[34] was applied by the Vienna *ab initio* simulation package[35] (VASP). As a simulation model of the 90°-domain

structure we used an orthorhombic supercell of $Pb_{12}Ti_{12}O_{36}$ that corresponds to $6\sqrt{2}\times\sqrt{2}\times1$ tetragonal $PbTiO_3$ units as modeled by Meyer and Vanderbilt in Ref. 36. The dimensions of the starting supercell and the fractional coordinates of the constituent ions were determined on the basis of the structural data[37] of $PbTiO_3$ at 300 K. The structural optimizations were performed within $Pmc2_1$ symmetry, where the polarization vectors of the $PbTiO_3$ units lay in the y-z plane. In the supercell, two 90° DWs are present parallel to the x-y plane. A cut-off energy of 400 eV and a k-point sampling grid of $4\times3\times1$ were adopted.

We first obtained an optimized supercell of the 90° DWs by carrying out the complete structural optimization of the starting supercell. Then, by using the optimized supercell, we prepared the 90° domain structures containing vacancies of Pb or O in order to investigate the interaction between the vacancies and the 90° DWs. In the supercell of $Pb_{12}Ti_{12}O_{36}$ with $Pmc2_1$ symmetry, all the constituent ions were positioned on the planes of $x=0$ or 1/2 with a site multiplicity of two. That is, there were two equivalent ions in the supercell. Therefore, the $Pb_{12}Ti_{12}O_{36}$ supercell consisted of eighteen symmetrically different O ions and six symmetrically different Pb ions. For the modeling of the O-vacancy-containing supercell, two O ions at a symmetrically equivalent site were extracted from the optimized supercell. The O-vacancy-containing cells ($Pb_{12}Ti_{12}O_{34}$) were subjected to partial relaxation of the first- and second-nearest-neighbor ions around the vacancies within $Pmc2_1$ symmetry. Pb-vacancy-containing cells ($Pb_{10}Ti_{12}O_{36}$) were prepared and subjected to partial relaxation in the same manner.

Calculations of the total energy (E_{total}) of the vacancy-containing cell ($Pb_{12}Ti_{12}O_{34}$ and $Pb_{10}Ti_{12}O_{36}$) were conducted after the partial relaxation around the vacancies. By comparing the E_{total} with the vacancies in different positions, the stabilization energies of the 90° DWs induced by O vacancy and Pb vacancy were evaluated.

IV. RESULTS AND DISCUSSION

A. PFM observations of domain-switching behavior in BiT crystals

Figure 1 shows a PFM image observed on the $a(b)$-c surface [Fig. 1(a)] and the a-b surfaces [Fig. 1(b)] of the standard BiT crystals after poling treatment. The out-of-plane PFM image in the $a(b)$-c surfaces [Fig. 1(a)] reveals that a single-domain state was not established even after a much higher E (100 kV/cm) than the coercive field (E_c) of 32 kV/cm was applied in the poling treatment. A larger part of the crystals had a P_s parallel to the poling direction [the bright-colored domains in Fig. 1(a)], which indicates that the P_s in this part was switched by the poling treatment. Hereafter, the part with P_s parallel to the poling direction will be referred to as "switched domains." Along with the switched domains, unswitched 90° domains (the domains surrounded by dotted lines) with P_s normal to the poling direction were found in the poled crystals. In addition, 180° domains, i.e., the domains with P_s antiparallel to the poling direction [the dark-colored domains in Fig. 1(a)] were also observed in this PFM image.

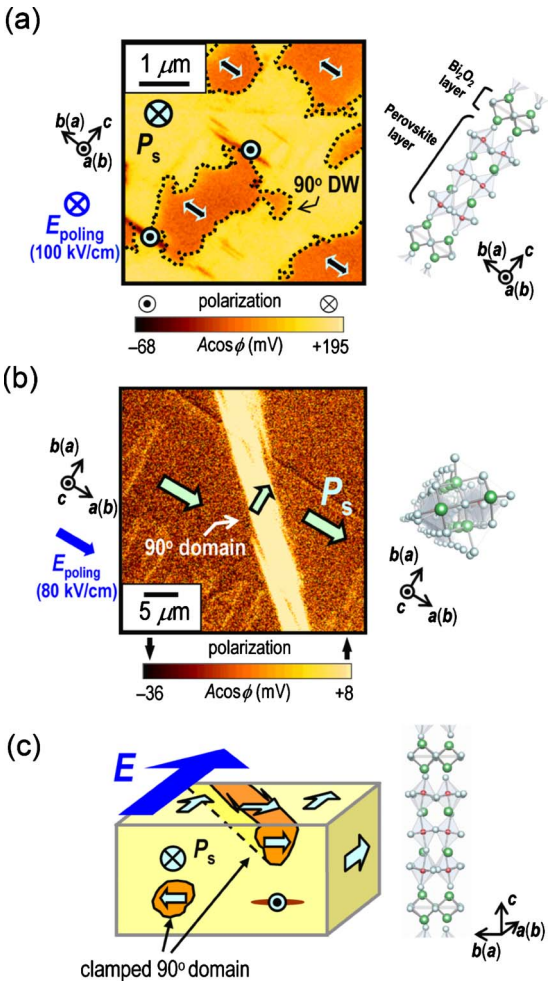

FIG. 1. (Color online) (a) Out-of-plane PFM image on the $a(b)$-c surface and (b) in-plane PFM image on the a-b surface of the standard BiT crystals (grown in air and annealed in air) after poling treatment. (c) Schematic three-dimensional domain structure of BiT after poling treatment. Poling treatment was conducted by applying a high electric field of 80–100 kV/cm along the $a(b)$ axis at 25 °C. The crystal structures shown in the figures in this paper were drawn with the 3D visualization software VESTA (Ref. 48).

Figure 1(b) shows an in-plane PFM image on the a-b surface of the standard BiT crystals after poling treatment with an E of 80 kV/cm along the $a(b)$ axis. As can be observed on the $a(b)$-c surfaces, an unswitched 90° domain was found on the a-b surfaces, manifesting as a bright-colored part in the middle of the image. Faceted (straight) 90° DWs were observed on the a-b surface of the BiT crystals before poling treatment (not shown)[32,38] while partially curved 90° DWs were detected on the a-b surface of the poled crystals. Using these PFM observations we are able to create a schematic three-dimensional domain structure in the poled BiT crystals, as shown in Fig. 1(c). Although the P_s vector in the larger part of the crystals was switched, the 90° DWs were strongly clamped, even after the application of an E that was much higher than E_c. The value of P_r is expressed by the following equation:

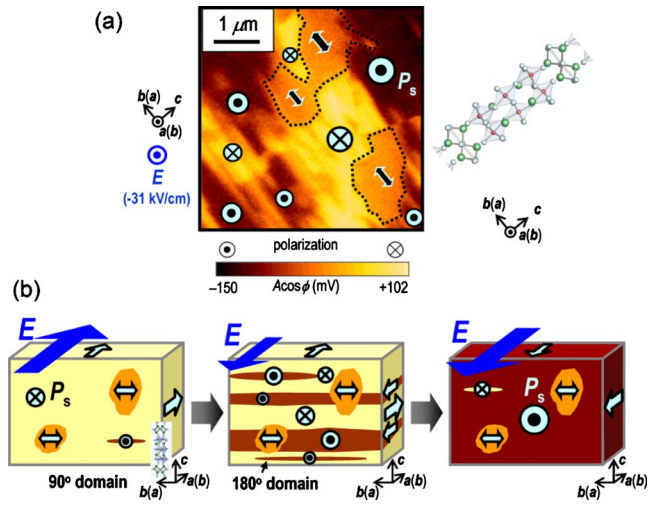

FIG. 2. (Color online) (a) Out-of-plane PFM image on the $a(b)$-c surface of a poled BiT crystal (a standard one) after application of an electric field of 30 kV/cm antiparallel to the poling direction. (b) Schematic domain dynamics during polarization switching in BiT single crystals.

$$P_r = (1 - F_{90^\circ\ \mathrm{domain}} - 2F_{180^\circ\ \mathrm{domain}})P_s, \qquad (2)$$

where $F_{90^\circ\ \mathrm{domain}}$ and $F_{180^\circ\ \mathrm{domain}}$ are the volume fractions of the clamped 90° domains and antiparallel 180° domains, respectively. Since $F_{90^\circ\ \mathrm{domain}}$ is much larger than $F_{180^\circ\ \mathrm{domain}}$ [see Fig. 1(c)], the clamping of 90° domains is proved to be responsible for the low P_r in BiT crystals.

Figure 2(a) shows an out-of-plane PFM image on the $a(b)$-c surfaces of the standard BiT crystals in which the poled domain structure [Fig. 1(c)] was partly switched by the following procedure: a high E of 100 kV/cm was applied along the $a(b)$ axis of the crystals as the poling treatment and then a moderate E of 31 kV/cm was applied in the direction antiparallel to the poling direction. Since the amplitude of the antiparallel E (31 kV/cm) is comparable to that of E_c (32 kV/cm), a partially switched domain structure appears in Fig. 2(a). While the 180° domains (dark-colored parts) grew markedly in Fig. 2(a) as compared to the poled domain structure in Fig. 1(a), a significant difference in the form and size of the 90° domains was not observed either before [Fig. 1(a)] or after [Fig. 2(a)] the application of an antiparallel E.

Figure 2(b) schematizes the domain-switching behavior in the standard BiT crystals. The comparison between the poled domain structure [Fig. 1(a)] and the partially switched domain structure [Fig. 2(a)] indicates that polarization switching of BiT is achieved by the growth of 180° domains. It is interesting to note that the growth of the 180° domains proceeds markedly on the a-b plane compared to the growth along the c axis. This may be attributed to the Bi_2O_2 layers or stacking faults along the c axis, which act as a barrier to the growth of the 180° domains. In addition, no significant difference is found between unswitched 90° domains shown in Figs. 1(a) and 2(a). This result strongly suggests that these 90° domains remained clamped during the polarization switching induced by the application of much a higher E (100 kV/cm) than E_c (32 kV/cm). We therefore conclude that

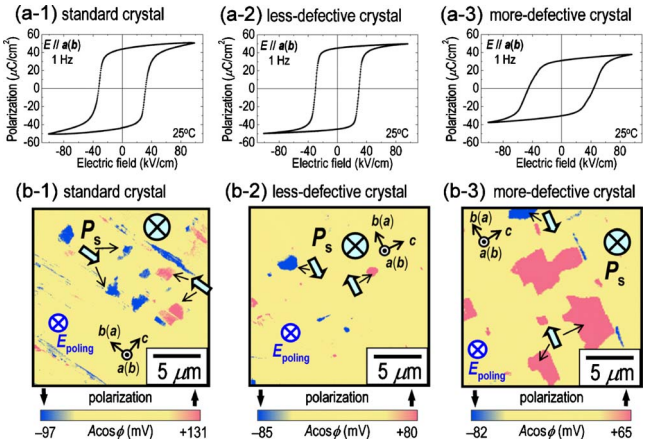

FIG. 3. (Color online) Polarization hysteresis loops [Figs. 3(a-1)–3(a-3)] and in-plane PFM images on the $a(b)$-c surfaces after poling treatment [Figs. 3(b-1)–3(b-3)] of three grades of BiT crystals: standard crystals [Figs. 3(a-1) and 3(b-1)], less-defective crystals [Figs. 3(a-2) and 3(b-2)] and more-defective crystals [Figs. 3(a-3) and 3(b-3)].

polarization switching is achieved by the growth of 180° domains while some 90° domains remain clamped in BiT crystals.

Figures 3(a-1)–3(a-3) show the polarization properties of the standard, less-defective, and more-defective BiT crystals. While the standard crystals showed a P_r of 43 $\mu C/cm^2$ [Fig. 3(a-1)], the less-defective crystals had a larger P_r of 45 $\mu C/cm^2$ [Fig. 3(a-2)]. This result indicates that a higher Po_2 during crystal growth enhances polarization properties, which is consistent with the results previously reported.[29,30] The more-defective crystals, in which the vacancy formation was promoted by the defect-formation treatment in nitrogen, exhibited a smaller P_r of 30 $\mu C/cm^2$ [Fig. 3(a-3)].

Figures 3(b-1)–3(b-3) show the in-plane PFM images on the $a(b)$-c surfaces of three grades of poled crystals: standard crystals [Fig. 3(b-1)], less-defective crystals [Fig. 3(b-2)], and more-defective crystals [Fig. 3(b-3)]. Since only the 90° domains with P_s normal to the poling direction appear in the in-plane PFM signals for the poled crystals, the in-plane PFM observations can be used to visualize the clamped 90° domains remaining after the poling treatment. These PFM observations reveal that the clamped 90° domains were enlarged, i.e., $F_{90^\circ\ \mathrm{domain}}$ increased in the BiT crystals exhibiting a lower P_r [see also Figs. 3(a-1)–3(a-3)].

Here we discuss the formation of clamped 90° domains in the poled BiT crystals. As shown in Fig. 3, more defective crystals with a higher $[V'''_{Bi}]$ and $[V^{\bullet\bullet}_{O}]$ showed an increase in $F_{90^\circ\ \mathrm{domain}}$ and a resultant lower P_r. This result suggests that the vacancies in the crystals are strongly associated with the clamping of 90° domains. As shown in Fig. 1(c), the clamped 90° domains have a needlelike shape along the ⟨110⟩ direction and have irregularly curved DWs. The configuration of these irregularly curved 90° DWs has a large energy compared with that of a faceted 90° DW parallel to the (110) plane,[39–41] as can be observed in certain perovskite-type ferroelectrics such as $BaTiO_3$ (Ref. 42) and $PbTiO_3$.[43] It has been reported in Ref. 32 that irregularly curved 90° DWs are formed as a result of their interaction with O vacancies, a

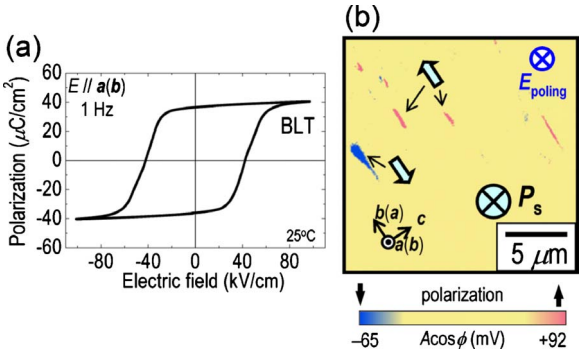

FIG. 4. (Color online) (a) Polarization hysteresis loop of BLT single crystals grown in air and annealed in air. (b) In-plane PFM image of the $a(b)$-c surface of a poled BLT single crystal.

subject which will be discussed later in detail.

We have also investigated the domain dynamics in BLT crystals. The substitution of La for BiT is well known to be an effective defect-control measure to enhance polarization properties and fatigue endurance in the forms of thin films[20] and ceramics.[21] Since the vacancy formation in BLT is suppressed by the strong bonding between A-site cations (La ions) and oxygen ions,[44] one can expect clamped 90° domains to be reduced in BLT crystals, as was observed in the less-defective BiT crystals. Figure 4(a) shows the polarization hysteresis loop of BLT crystals. Although the BLT crystals exhibited a well-saturated hysteresis loop, the value of P_r (36 $\mu C/cm^2$) was smaller than that of the standard BiT crystals (43 $\mu C/cm^2$). Figure 4(b) shows an in-plane PFM image of the $a(b)$-c surfaces of the BLT crystals after poling treatment, which visualizes the clamped 90° domains. Compared with the standard BiT crystals [Fig. 3(b-1)], the volume fraction of the clamped 90° domains was clearly reduced, and polarization switching was achieved in almost the entirety of each BLT crystal. These results also indicate that the smaller P_r observed in the BLT crystals can be attributed not to domain clamping but to the smaller P_s (Ref. 31) of BLT. It is suggested that the larger P_r reported for ceramics and thin films of BLT can be attributed to a reduction in the clamped 90° domains beyond the disadvantage of the smaller P_s.

B. *Ab initio* calculations of the interaction between the vacancies and 90° DWs

Figure 5(a) exhibits the 90° domain structure of $PbTiO_3$ after structural optimization of the $Pb_{12}Ti_{12}O_{36}$ supercell and Fig. 5(b) depicts the P_s vector of each perovskite $PbTiO_3$ unit. In this study, we define a $PbTiO_3$ unit as a Ti-centered unit with six neighboring O shared by two units and the eight neighboring Pb ions shared by eight units. The P_s vector of the $PbTiO_3$ unit, $\mathbf{P}_s$, is evaluated by

$$\mathbf{P}_s = \sum_j (w_j \times Q_j e \times \mathbf{u}_j)/\Omega, \tag{3}$$

where the index j runs through all the constituent ions of the perovskite unit, w_j is the weight factor (1/8 for Pb, 1 for Ti, and 1/2 for O), Q_j is the valence number, e is the elementary

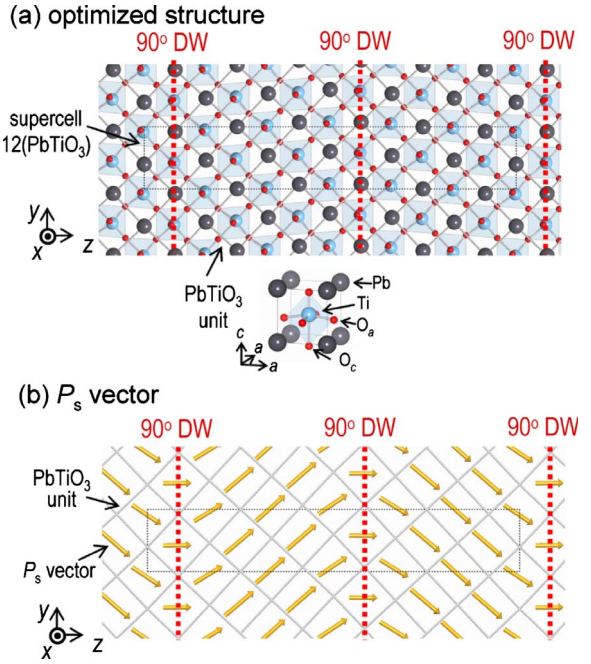

FIG. 5. (Color online) (a) 90° domain structure after full atomic relaxation and (b) P_s vector of each perovskite $PbTiO_3$ unit in the 90° domain structure.

charge, $\mathbf{u}_j$ is the displacement vector from the ideal cubic (nonpolar) position of each ion, and Ω is the volume of each perovskite unit. Here, the formal charge (+4 for Ti, +2 for Pb, and −2 for O) is adopted as Q_j. The structural optimization yields a reasonable 90°-domain structure where the maximal angle of $\mathbf{P}_s$ with the z axis is 41.9°, which is in good agreement with the 40.4° reported in Ref. 36. In this study we define the position of 90° DWs as the z planes passing through the Ti ions (Pb-Ti-O planes) in which the angle that $\mathbf{P}_s$ forms with the z axis is almost zero (0.5°). The 90° DWs are shown as dashed lines in Figs. 5(a) and 5(b).

Figure 6(a) presents the detailed crystal structure around the 90° DW in the optimized supercell. The tetragonal $PbTiO_3$ has two kinds of O: O_c and O_a. These oxygen atoms are determined by whether the bond between the O and the adjacent Ti is along the c axis (O_c) or the a axis (O_a) in the tetragonal unit cell. O_c has one short bond with the adjacent Ti while O_a has two intermediate Ti-O bonds. The O_c and O_a are distinguished in the supercell of the 90° DW in the same manner. In addition, there are two kinds of O_a in the 90° domain structure: one is on the Pb-Ti-O plane [O_a^* unmarked in Fig. 6(a)] and the other is on the O-O plane parallel to the 90° DW [O_a marked in Fig. 6(a)]. An extremely larger supercell along the x axis is required in order to properly calculate the E_{total} for the O_a^* vacancies. The E_{total} for the O_a^* vacancies is overestimated for the supercell adopted in this study because Ti has to have two neighboring O_a^* vacancies in this supercell. Thus the O_a^* vacancies are ruled out in our calculations.

Figure 6(b) shows the relative E_{total} with respect to the distance of the O vacancies from the 90° DW. The calculations show that the supercells with O vacancies near the 90° DW have a lower relative E_{total}. Note that the minimum of

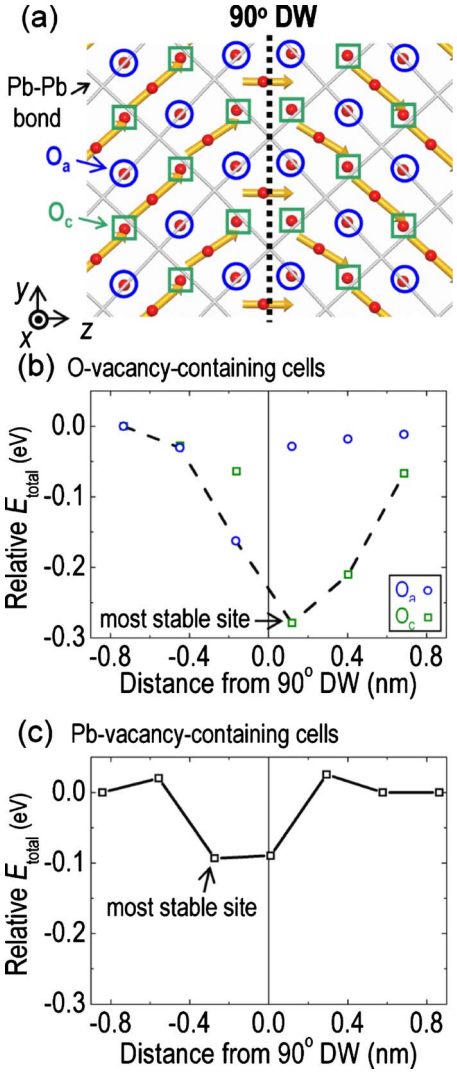

FIG. 6. (Color online) (a) Detailed structure and polarization direction around the 90° DW with oxygen sites divided into three groups, and relative E_{total} of (b) O-vacancy-containing and (c) Pb-vacancy-containing cells as a function of the distance between the vacancy site and the 90° DW.

the relative E_{total} is found to lie at the adjacent O_c site at a distance of 0.1 nm from the 90° DW. The stabilization energy of the 90° DW induced by the O vacancy, corresponding to the depth of the minimum in the energy curve shown in Fig. 6(b), is calculated to be 0.27 eV/cell (0.13 eV/vacancy). Meyer and Vanderbilt[36] have reported that the energy barrier for the motion of 90° DW in defect-free $PbTiO_3$ crystals evaluated in their DFT calculations is less than 1.6 mJ/m^2, which corresponds to 4.4×10^{-3} eV/cell. The stabilization energy of the 90° DW induced by the O vacancy (0.27 eV/cell) is much higher than 4.4×10^{-3} eV/cell for the energy barrier for the motion of 90° DWs without O vacancy. These calculation results indicate that a 90° DW is stabilized by the adjacent O vacancies at the O_c site.

Figure 6(c) shows the relative E_{total} for the Pb-vacancy-containing supercells. The results exhibit a slightly lower value for the relative E_{total} when the Pb vacancy neighbors are near to the 90° DW. The stable site of the Pb vacancy was found to be at or on the left side of the 90° DW as indicated in Fig. 6(c). The stabilization energy of the Pb vacancy is estimated to be 0.09 eV/cell (0.04 eV/vacancy), which is much smaller than that of the O vacancy.

It is interesting to note that the stable sites for the vacancies of O and Pb are positioned on the different sides of the 90° DW. The O vacancies are positively charged while the Pb vacancies are negatively charged in the lattice. These results suggest that one of the major origins of the stabilization of the 90° DW by the adjacent vacancies is an electrostatic interaction between the charge in the vacancies and the electrostatic potential modulated across the 90° DW. Theoretical calculations[36,45] have shown that the component of $\mathbf{P}_s$ normal to 90° DWs is smaller at the 90° DWs than it is inside the bulk crystals. The decrease in the $\mathbf{P}_s$ component leads to a modulation of the electrostatic potential, according to Poisson's equation, so that an electric field produced by the partial differentiation of the electrostatic potential is built in across the 90° DW. This built-in electric field near the 90° DW has been reported to be as high as 1 MV/cm for $BaTiO_3$.[46] The modulation of the electrostatic potential near the 90° DW yields an attractive interaction with the charged vacancies. Positively and negatively charged species energetically prefer to reside at the maximum and minimum sites of the electrostatic potential near the 90° DWs, respectively. This electrostatic interaction provides the stable sites of the vacancies of O and Pb adjacent to but on different sides of the 90° DW. Our calculations of $\mathbf{P}_s$ [see Fig. 5(b)] show that the component of $\mathbf{P}_s$ along the z axis is suppressed at the 90° DWs by 1.2 $\mu C/cm^2$, which is comparable with the value reported in Ref. 36. This suppression of the $\mathbf{P}_s$ component results in a local modulation of the electrostatic potential near the 90° DW. The attractive interaction between the defect charge and the electrostatic potential modulation is considered one of the major origins of the stabilization of the 90° DW by O vacancies.

The O-vacancy-containing supercells in this study have a much high concentration of O vacancy (approximately 5.6%) than real ferroelectric oxide. For real $PbTiO_3$, the maximal concentration of O vacancy has been reported to be 3.3%,[47] and the actual concentration of O vacancy is considered to be around 1%. However, oxygen vacancies can diffuse with random walk because they have sufficient mobility to migrate, even at room temperature. Furthermore, the migration of oxygen vacancies is accelerated by the application of an electric field during polarization switching. If an O vacancy gets within an effective range of the attractive interaction from 90° DW once, the O vacancy can readily find the most stable site adjacent to the 90° DW. The O vacancy is then trapped and cannot easily escape from the stable site. In addition, O vacancies can accumulate and form a defect plane at the 90° DW because 90° DWs have a stable site of O vacancy in each $PbTiO_3$ unit cell. These 90° DWs, coupled with a defect plane composed of O vacancies, are expected to be strongly clamped and can no longer be moved through the application of an electric field.

C. Interaction between the O vacancies and 90° DWs in the BiT system

Here we discuss the origin of 90°-domain clamping observed in BiT crystals. From the calculated results for

$PbTiO_3$, a similar interaction between 90° DWs and O vacancies is also suggested for BiT as well. The component of $\mathbf{P}_s$ normal to the 90° DW for $PbTiO_3$ [see Fig. 5(b)] is suppressed at the 90° DW, an effect which is caused mainly by the strain caused by the vending of $\mathbf{P}_s$ across the 90° DW. The suppression of the $\mathbf{P}_s$ component leads to a modulation of the electrostatic potential. Because 90° DWs in BiT should have a similar modulation of electrostatic potential, the stable sites of O vacancies are present near the 90° DWs for BiT as well.

The formation energy of O vacancies differs in the Bi_2O_2 and the perovskite layers because BiT crystals are composed of a regular stacking of the Bi_2O_2 layers and the perovskite layers of $Bi_2Ti_3O_{10}$. High-resolution synchrotron x-ray and neutron-diffraction analyses show that O vacancies are abundant in the perovskite layers.[29] These results show that the stable sites of O vacancies are mainly in the perovskite layers due to the weak bonding between Bi at the *A* site and O. A high concentration of O vacancies provides high oxide-ion conduction in BiT single crystals in the *a*-*b* plane, which indicates the presence of a fast diffusion path of O vacancies in the perovskite layers.[28] This fast diffusion path of O vacancies enhances the accumulation of O vacancies near 90° DWs, which then lead to the clamping of the 90° DWs in BiT crystals.

Another factor that may contribute to the strong clamping of 90° DWs is the high T_C of 675 °C for BiT. In the temperature range from T_C to about 400 °C, O vacancies in the perovskite layers can migrate much faster than they can at room temperature. Therefore, the probability that O vacancies get within an effective range of the attractive interaction from 90° DWs becomes high at high temperatures. As a result, a high concentration of O vacancies accumulates near 90° DW and the 90° DWs are strongly clamped by O vacancies.

At high temperatures below T_C, not only O vacancies but also 90° DWs have high mobility in BiT crystals. The interaction between O vacancies and 90° DWs is considered to affect the domain structure and the clamping of 90° DWs. As described above, the oxide-ion conductivity of BiT crystals is much higher in the *a*-*b* plane than along the *c* axis and the movement of the 90° DWs along the *a*(*b*) axis then becomes viscous due to the interaction with O vacancies. When the crystals are cooled to room temperature, the complicated structures of the 90° DWs are frozen before flat (faceted) 90° DWs with the (110) plane are developed throughout the crystals as observed in as-grown BiT crystals.[32] It is likely that some parts of the 90° DWs in the cooled crystals have already been clamped before the poling treatment due to a local accumulation of O vacancies in the 90° DWs at high temperatures below T_C. The migration of O vacancies during cooling at high temperatures and in the subsequent domain switching induced by the application of an electric field at room temperature leads to a complicated structure of the clamped 90° domains observed in the poled crystals [see in Figs. 1–3].

One indirect way to verify the influence of O vacancies on the clamping of 90° DWs is the quenching of BiT at high temperatures above T_C. If the samples are quenched by high temperatures above T_C to room temperature, the clamping strength of 90° DWs by O vacancies can be expected to be reduced because of the low probability that the O vacancies will meet 90° DWs. Noguchi *et al.*[21] have reported that the value of P_r in BiT ceramics quenched at 800 °C in an N_2 atmosphere was almost twice as large as that of BiT ceramics that were slowly cooled in air. In addition, BiT ceramics quenched at 800 °C in an O_2 atmosphere exhibited almost the same P_r as those quenched at 800 °C in an N_2 atmosphere. These results clearly show that the clamping of 90° DWs by O vacancies is governed not only by the total concentration of O vacancies but also by the diffusion process of O vacancies below T_C. The marked influence of the diffusion process of O vacancies suggests that the concentration of O vacancies near 90° DWs determines the clamping strength of the 90° DWs. It is concluded that the strong attractive interaction with O vacancies is the origin of the domain clamping of 90° DWs in the BiT system.

V. CONCLUSIONS

The structure and clamping of ferroelectric domains in single crystals of BiT and BLT were investigated through polarization measurements along the *a*(*b*) axis and PFM. It has been shown that polarization switching is achieved by the growth of 180° domains and that unswitched 90° domains with clamped DWs lead to a low remanent polarization. The formation of the vacancies of Bi and O in BiT crystals at high temperatures increased the volume fraction of the clamped 90° domains and thereby lowered the remanent polarization. BLT crystals exhibited a remarkable decrease in the volume fraction of the clamped 90° domains, which we suggest may be responsible for the superior polarization properties observed in BLT ceramics and films. *Ab initio* calculations of $PbTiO_3$ showed that oxygen vacancy is stabilized adjacent to the 90° DW by 0.13 eV/vacancy mainly due to an attractive interaction between an electrostatic potential modulation near the 90° DW and O vacancies. A large stabilization energy of oxygen vacancies near 90° DWs, along with the high mobility of oxygen vacancies along the *a*-*b* plane, was suggested to be the origin of the strong clamping of 90° DWs in BiT crystals. It is concluded that the clamping of 90° DWs in BiT originates from a strong attractive interaction with the oxygen vacancies trapped at stable sites adjacent to the 90° DWs.

ACKNOWLEDGMENTS

This study was partly supported by a Grant-in-Aid for Scientific Research on Priority Areas "Novel States of Matter Induced by Frustration" (Grant No. 19052002), the Fundamental R&D Program for Core Technology of Materials funded by the Ministry of Knowledge Economy, Republic of Korea, and a Grant-in-Aid for Research Fellows of the Japan Society for the Promotion of Science (Grant No. 08J09794).

[1] D. Feng, N.-B. Ming, J.-F. Hong, Y.-S. Yang, J.-S. Zhu, Z. Yang, and Y.-N. Wang, Appl. Phys. Lett. **37**, 607 (1980).
[2] S.-E. Park and T. R. Shrout, J. Appl. Phys. **82**, 1804 (1997).
[3] S. Wada, S. Suzuki, T. Noma, T. Suzuki, M. Osada, M. Kakihana, S. E. Park, L. E. Cross, and T. R. Shrout, Jpn. J. Appl. Phys. **38**, 5505 (1999).
[4] L. M. Eng, Nanotechnology **10**, 405 (1999).
[5] M. E. Drougard and D. R. Young, Phys. Rev. **94**, 1561 (1954).
[6] U. Robels and G. Arlt, J. Appl. Phys. **73**, 3454 (1993).
[7] V. Nagarajan, A. Roytburd, A. Stanishevsky, S. Prasertchoung, T. Zhao, L. Chen, J. Melngailis, O. Auciello, and R. Ramesh, Nature Mater. **2**, 43 (2003).
[8] J. F. Scott and C. A. Paz de Araujo, Science **246**, 1400 (1989).
[9] H. M. Duiker, P. D. Beale, J. F. Scott, C. A. P. de Araujo, B. M. Melnick, J. D. Cuchiaro, and L. D. McMillan, J. Appl. Phys. **68**, 5783 (1990).
[10] P. V. Lambeck and G. H. Jonker, J. Phys. Chem. Solids **47**, 453 (1986).
[11] D. C. Lupascu, Y. A. Genenko, and N. Balke, J. Am. Ceram. Soc. **89**, 224 (2006).
[12] W. L. Warren, D. Dimos, G. E. Pike, B. A. Tuttle, M. V. Raymond, R. Ramesh, and J. T. Evans, Appl. Phys. Lett. **67**, 866 (1995).
[13] J. F. Scott and M. Dawber, Appl. Phys. Lett. **76**, 3801 (2000).
[14] M. Dawber and J. F. Scott, Appl. Phys. Lett. **76**, 1060 (2000).
[15] L. He and D. Vanderbilt, Phys. Rev. B **68**, 134103 (2003).
[16] M. Calleja, M. T. Dove, and E. K. H. Salje, J. Phys.: Condens. Matter **15**, 2301 (2003).
[17] S. E. Cummins and L. E. Cross, J. Appl. Phys. **39**, 2268 (1968).
[18] A. D. Rae, J. G. Thompson, R. L. Withers, and A. C. Willis, Acta Crystallogr., Sect. B: Struct. Sci. **46**, 474 (1990).
[19] P. C. Joshi and S. B. Krupanidhi, Appl. Phys. Lett. **62**, 1928 (1993).
[20] B. H. Park, B. S. Kang, S. D. Bu, T. W. Noh, J. Lee, and W. Jo, Nature (London) **401**, 682 (1999).
[21] Y. Noguchi, I. Miwa, Y. Goshima, and M. Miyayama, Jpn. J. Appl. Phys. **39**, L1259 (2000).
[22] Y. Noguchi and M. Miyayama, Appl. Phys. Lett. **78**, 1903 (2001).
[23] Y. Noguchi, M. Soga, M. Takahashi, and M. Miyayama, Jpn. J. Appl. Phys. **44**, 6998 (2005).
[24] H. Nagata, J. Ceram. Soc. Jpn. **116**, 271 (2008).
[25] N. H. Chan, R. K. Sharma, and D. M. Smyth, J. Am. Ceram. Soc. **64**, 556 (1981).
[26] J. Chen, M. P. Harmer, and D. M. Smyth, J. Appl. Phys. **76**, 5394 (1994).
[27] M. V. Raymond and D. M. Smyth, J. Phys. Chem. Solids **57**, 1507 (1996).
[28] M. Takahashi, Y. Noguchi, and M. Miyayama, Jpn. J. Appl. Phys. **41**, 7053 (2002).
[29] Y. Noguchi, T. Matsumoto, and M. Miyayama, Jpn. J. Appl. Phys. **44**, L570 (2005).
[30] K. Yamamoto, Y. Kitanaka, M. Suzuki, M. Miyayama, Y. Noguchi, C. Moriyoshi, and Y. Kuroiwa, Appl. Phys. Lett. **91**, 162909 (2007).
[31] M. Soga, Y. Noguchi, M. Miyayama, H. Okino, and T. Yamamoto, Appl. Phys. Lett. **84**, 100 (2004).
[32] S. Katayama, Y. Noguchi, and M. Miyayama, Adv. Mater. **19**, 2552 (2007).
[33] D. C. Langreth and J. P. Perdew, Phys. Rev. B **21**, 5469 (1980).
[34] P. E. Blöchl, Phys. Rev. B **50**, 17953 (1994).
[35] G. Kresse and J. Hafner, Phys. Rev. B **49**, 14251 (1994).
[36] B. Meyer and D. Vanderbilt, Phys. Rev. B **65**, 104111 (2002).
[37] Y. Kuroiwa, S. Aoyagi, A. Sawada, J. Harada, E. Nishibori, M. Takata, and M. Sakata, Phys. Rev. Lett. **87**, 217601 (2001).
[38] Y. Kitanaka, Y. Noguchi, and M. Miyayama, Appl. Phys. Lett. **90**, 202904 (2007).
[39] J. Fousek and V. Janovec, J. Appl. Phys. **40**, 135 (1969).
[40] Y. Ishibashi and M. Iwata, Jpn. J. Appl. Phys. **46**, 272 (2007).
[41] M. Iwata, Y. Morishita, R. Aoyagi, M. Maeda, I. Suzuki, and Y. Ishibashi, Jpn. J. Appl. Phys. **46**, 3485 (2007).
[42] W. J. Merz, Phys. Rev. **95**, 690 (1954).
[43] J. Kobayashi, J. Appl. Phys. **29**, 866 (1958).
[44] S. J. Kim, C. Moriyoshi, S. Kimura, Y. Kuroiwa, K. Kato, M. Takata, Y. Noguchi, and M. Miyayama, Appl. Phys. Lett. **91**, 062913 (2007).
[45] Y. Xiao, V. B. Shenoy, and K. Bhattacharya, Phys. Rev. Lett. **95**, 247603 (2005).
[46] Q. Zhang and W. A. Goddard, Appl. Phys. Lett. **89**, 182903 (2006).
[47] R. L. Holman and R. M. Fulrath, J. Appl. Phys. **44**, 5227 (1973).
[48] K. Momma and F. Izumi, J. Appl. Crystallogr. **41**, 653 (2008).